# EVALUATION ON DISCRETE SOURCE DAMAGES OF CFRP STIFFENED PANELS

**Yuichiro Aoki, Shin-ichi Takeda, Hirokazu Shoji, Sunao Sugimoto and Yutaka Iwahori**
**Japan Aerospace Exploration Agency**
*aoki.yuichiro@jaxa.jp; takeda.shinichi@jaxa.jp; shoji.hirokazu@jaxa.jp; sugimoto.sunao@jaxa.jp; iwahori.yutaka@jaxa.jp*

**Keywords**: *Composite structure, engine debris uncontained event, large notch damage, damage tolerance, progressive failure analysis*

## Abstract

*Engine debris penetration tests were conducted to evaluate the large notch damage and residual strength of composite stiffened panel. The damage mechanism was examined by progressive failure analysis based on Hashin's failure criteria and cohesive zone model. The influence of delamination on the progressing notched damage path and initial failure load of the panel are investigated. The results reveal that typical damage path is characterized by fiber breakage perpendicular to the crack tips to be followed by skin/stringer interface damage. The numerical model has a potential capability to predict the debris penetration and residual strength of the damaged panel.*

## 1 Introduction

Recently, composite materials are successfully used in primary aircraft structures such as wing, fuselage, and empennage. In operational aspect, engine debris uncontained events have long been recognized as a major threat for airplane safety in the commercial transport fleet. Therefore, damage tolerance capabilities on penetration and large notch damages are stringently evaluated by both tests and analysis [1-4]. In particularly, fuselage is the most critical part for such kind of damages because the structures are predominantly thin-walled components and has greater potential risk of severe uncontained damage. One of the legacy design requirements is a damage-tolerance capability to a two-bay crack. The two-bay crack represents a discrete source damage caused by fragments from a failed engine, which spans from one bay to the other bay. This requirement is originally applied to conventional metallic structures with the analytical consideration of crack propagation based on stress intensity factor solutions. Composite structure is essentially different from metallic structure in terms of damage modes and fracture behaviors. Major damages in composite structures are delaminations with matrix cracks and fiber breakages. Composites materials have anisotropic and heterogeneous properties whilst metal material is isotropic and homogeneous. Therefore, it is difficult to apply directly fracture mechanics to the two-bay crack problem in composite structure. More fundamental knowledge on discrete source damage of composite fuselage structure is needed to understand the damage tolerance capabilities of composite fuselage structures.

In this paper, a two-bay crack was introduced into the composite panel with 3 hat-shaped stringers by an artificial engine debris penetration test. The damage configuration was evaluated by non-destructive inspections. Then, residual strength tests were conducted to verify the damage-tolerance capabilities of the panels with such a discrete source damage including the two-bay crack. The numerical simulations are also implemented with commercial available code, which includes two damage progressive failure analysis methodologies based on intralaminar damage modes (fiber breakage and matrix cracking) and interlaminar damage mode (delamination).

## 2 Blade penetration test

### 2.1 Test panel

Size of test panel is 900 mm long x 750 mm width and their skin thickness is 2 mm. The layup of the panel and stringer is quasi-isotropic with fiber fraction of [0° / 90°/ ±45° = 25% / 25% / 50%]. The panels are fabricated in different material systems and fabrication processes; a unidirectional prepreg material with an autoclave method and dry fabrics with VaRTM (Vacuum-assisted resin transfer molding) process. Detailed specification of the panel is shown in Fig. 1 and Table 1. Total of two panels are prepared for each fabrication method. One panel is applied to both blade impact test and subsequent tensile strength test. The other one is machined to make an artificially ideal 200mm long two-bay crack at middle of the panel for the comparison of failure behavior under tensile load as shown in Fig. 2.

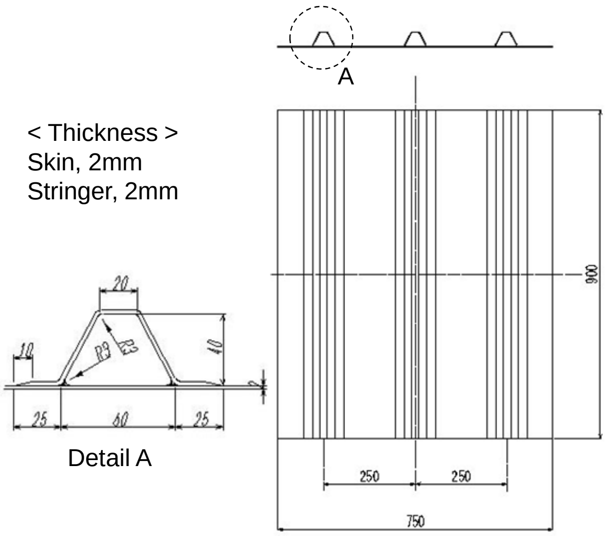


Fig. 1 Dimensions of test panel

Table 1 Material and layup

| Type | Fiber | Resin | Layup |
|---|---|---|---|
| Autoclave | UD prepreg, Q-111B 1240（STS-24K）<br>Toho Tenax Co. | | 16ply<br>$[45/0/-45/90]_{2s}$ |
| VaRTM | Biaxial-NCF（STS-24K）<br>SAERTEX | #6809<br>Nagase Chemtex Co. | 16ply<br>$[(45/-45)/(0/90)]_{2s}$ |

Fig. 2 Notched panel

### 2.2 Test setup

The blade penetration tests were conducted by a pneumatic high velocity impact testing machine in JAXA Chofu Aerospace Center (Fig. 3). Two composite panels mentioned above were impacted by Ti-6Al-4V titanium projectile shown as Fig. 4. The projectile is designed to simulate an uncontained fragment from a failed engine and has two sharp edges to certainly give severe penetration damage to the panel [5]. The total mass of the projectile is 195 g and target velocity is 200m/sec. The projectile is mounted in the front of sabot (Fig. 4), which will support the projectile in the barrel of the impact machine. The orientation of the projectile is controlled by careful design of the sabot. The major axis of the blade is aligned to the vertical plane in the required orientation for penetration in the target.

When the impact machine is fired, a rapid release of the pressurized air from the reservoir accelerates the sabot and projectile down the launch barrel. The velocity of the projectile is controlled by the initial charge of the air pressure in reservoir. At the exit of the barrel, the sabot is arrested by the stopper and the

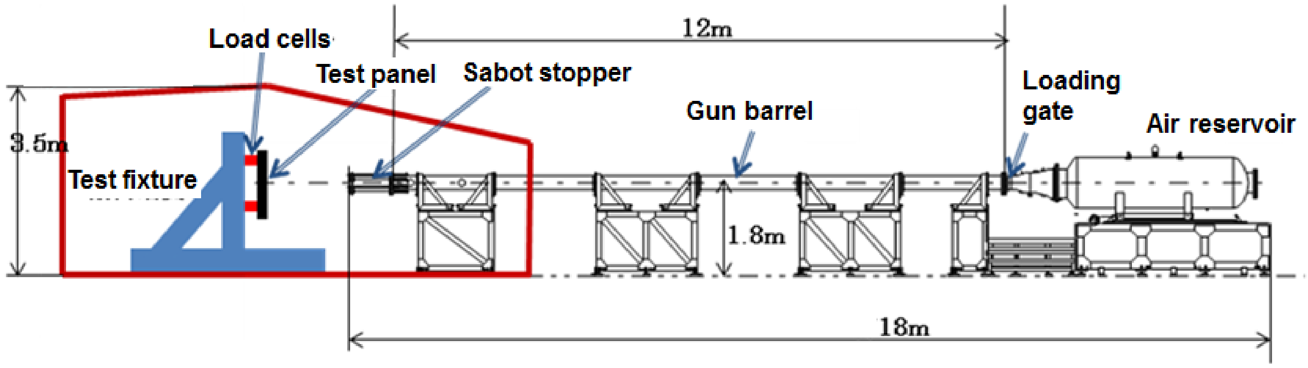


Fig. 3 Pneumatic high velocity impact testing machine

Fig. 4 Titanium projectile (Left: Overview, Right: Blade/sabot combination)

projectile completely separates from the sabot. A short distance of projectile free flight, typically 2 m, ensures that the orientation does not change and the projectile reaches the target at the required location.

Optical imaging of the projectile in free flight before the impact was made using high-speed cameras. These images are used to confirm that sabot separation has occurred successfully and that the projectile is stable in flight. Also, the images are used to determine the projectile velocity.

After each impact test, the composite panels were stored in a dry laboratory environment for detailed inspection and preparation of tensile test fixtures.

## 3 Progressive Failure Analysis

An analysis for predicting blade penetration damage and failure of damaged composite panel is implemented using a progressive damage analysis methodology within the ABAQUS/Explicit (version 6.10) finite element analysis code. The progressive failure analysis methodology includes intralaminar and interlaminar damage initiation and propagation. The intralaminar damages considered in this study are

a. Fiber failure in tension and compression
b. Matrix failure in tension and compression

The Hashin's unidirectional criteria [6-7] are used to predict intralaminar damage initiation, which criteria consider four different damage initiation mechanisms above.
The initiation criteria have the following general forms:

Fiber failure in tension:

$$F_f^t = \left(\frac{\sigma_{11}}{X^T}\right)^2 \quad for \quad \sigma_{11} \geq 0$$

Fiber failure in compression:

$$F_f^c = \left(\frac{\sigma_{11}}{X^C}\right)^2 \quad for \quad \sigma_{11} < 0$$

Matrix failure in tension:

$$F_m^t = \left(\frac{\sigma_{22}}{Y^T}\right)^2 + \left(\frac{\tau_{12}}{S^L}\right)^2 \quad for \quad \sigma_{22} \geq 0$$

Matrix failure in compression:

$$F_m^c = \left(\frac{\sigma_{22}}{2S^T}\right)^2 + \left[\left(\frac{Y^C}{2S^T}\right)^2 - 1\right] \cdot \frac{\sigma_{22}}{Y^C} + \left(\frac{\tau_{12}}{S^L}\right)^2$$

$$for \quad \sigma_{22} < 0$$

in the above equations , each symbol denotes:

$X^T$: Longitudinal tensile strength
$X^C$: Longitudinal compressive strength
$Y^T$: Transverse tensile strength
$Y^C$: Transverse compressive strength
$S^L$: Longitudinal shear strength
$S^T$: Transverse shear strength
$\sigma_{11}$, $\sigma_{22}$, $\tau_{12}$: In-plane stress components

Interlaminar damage is modeled using the ABAQUS generic cohesive element COH3D8 at the evaluated ply interface. The interlaminar damage model is defined in terms of bi-linear traction-separation constitutive law. The initiation of delamination is determined based on quadratic nominal stress criterion represented as

$$\left(\frac{\langle t_n \rangle}{t_n^0}\right)^2 + \left(\frac{t_s}{t_s^0}\right)^2 + \left(\frac{t_t}{t_t^0}\right)^2 = 1$$

where, $t^0{}_n$, $t^0{}_s$, $t^0{}_t$,denote the peak values of the nominal stress when the deformation is either purely normal to the interface or purely in the first or the second shear direction, respectively.
Delamination propagation is defined based on the energy that is dissipated as a result of the damage growth, i.e. fracture energy. The fracture energy is equal to the fracture toughness obtained from DCB test for mode I fracture toughness and ENF test for mode II toughness. The dependence of the fracture energy under mixed-mode condition is defined based on a power law fracture criterion. That is given by

$$\left(\frac{G_n}{G_{IC}}\right)^2 + \left(\frac{G_s}{G_{IIC}}\right)^2 + \left(\frac{G_t}{G_{IIIC}}\right)^2 = 1$$

where, $G_{IC}$, $G_{IIC}$ and $G_{IIIC}$ denote Mode I fracture toughness, Mode II fracture toughness and Mode III fracture toughness, respectively. The quantities $G_n$, $G_s$ and $G_t$ refer to the work done by the traction and its conjugate relative displacement in the normal, the first and the second shear directions, respectively. The unit for those quantities is represented by the energy per unit area. In this study, $G_{IIIC}$ is assumed to be the same value as $G_{IIC}$.
Three dimensional finite element model was developed to perform the progressive damage analysis using the ABAQUS/Explicit code as shown in Fig.5. The 8-node continuum shell element (SC8R) is used for modeling the skin panel and stringers with actual definition of stacking sequences, which enables predictions of intralaminar damage modes. The projectile is modeled using three-dimensional solid elements (C3D8R). The finite element model includes all area of the test panel generated by meshes of 5 mm wide and 5 mm long. The thickness of the panel is divided in to 2 sections connected with a cohesive layer with coincident nodes. The finite element model is a simplified to have a

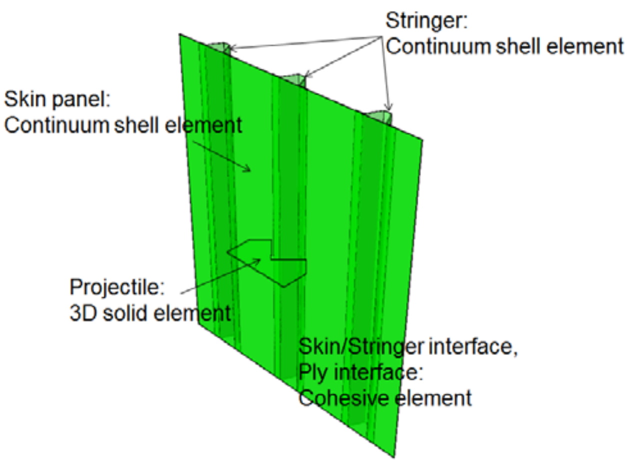


Fig. 5 Finite element model

single cohesive layer in the skin panel and in the interface between skin and stringer, where interlaminar damage in stringer was neglected. The thickness of each ply interface is assumed to be 0.025mm that is equivalent to 10% of lamina thickness. Therefore, cohesive layer in the skin and skin/stringer interface are respectively 0.375mm (15 interfaces) and 0.125mm (1 interface). The friction coefficient between panel and projectile is assumed to be 0.3. The projectile doesn't have sharp edges at two peaks because of modeling difficulties. However, the projectile has the same in-plane dimensions and initial kinetic energy as shown in tests. During the analysis, finite element is removed from the mesh when each damage criterion is satisfied at all of the through-the-thickness section points at any one integration location of an element. If an element is removed, it offers no resistance to subsequent deformation. All the material properties used in the analysis are shown in Table 2, 3 and 4

## 4 Result and discussions

### 4.1 Blade penetration test

The main damage was a large crack penetrating from one bay to the other bay, so-called two-bay crack condition, and its length was 200 mm as same as the projectile width. Fig. 6 shows the penetration damage and inspection result by ultrasonic C-scan. Some delaminations occurred at the edge of the two-bay crack with fiber breakages. The shape of the delamination in the panel by autoclave method was different from that in the panel by VaRTM.

After the penetration tests, residual tensile strength tests have been conducted using hydraulic testing machine. The failure behaviors of the panels were observed by a multi-channel strain measurement system and an AE (Acoustic emission) system and a digital video camera. The in-plane strain change was evaluated by DIC (Digital Image Correlation) technique. The damage propagated in the width direction and penetrated one adjacent stiffener with the load increase, and then debonding at another stringer was caused by out-of-plane deformation of the panel. The maximum load of the prepreg panel was about 320 kN before final failure of one stringer, and then the load dropped suddenly with another stringer failure. The final failure mode and load-displacement curve are shown in Fig. 7 and Fig. 8, respectively.

Table 2 Lamina properties

| $E_1$ (GPa) | $E_2$, $E_3$ (GPa) | $\nu_{12}$, $\nu_{13}$ | $G_{12}$, $G_{13}$ (GPa) | $G_{23}$ (GPa) |
|---|---|---|---|---|
| 130.1 | 8.03 | 0.31 | 4.8 | 2.69 |

Table 3 Strength for Hashin's criteria

| $X^T$(MPa) | $X^C$ (MPa) | $Y^T$ (MPa) | $Y^C$ (MPa) | $S^L$ (MPa) | $S^C$ (MPa) |
|---|---|---|---|---|---|
| 2864 | 1537 | 80 | 160 | 140 | 140 |

Table 4 Cohesive layer properties

| $G_{IC}$ (J/m$^2$) | $G_{IIC}$, $G_{IIIC}$ (J/m$^2$) | $S_I$ (MPa) | $S_{II}$, $S_{III}$ (MPa) |
|---|---|---|---|
| 0.98 | 1.47 | 40 | 100 |

### 4.2 Progressive failure analysis

The simulation results obtained from the progressive failure analysis of blade penetration for prepreg panel are presented in Fig. 9, in which, time denotes the duration from the beginning of blade penetration. The elements completely failed are removed from the mesh. Figure 10 shows the energy balance in the model, with kinetic energy, damage dissipation, strain and total internal energies in function of time. The kinetic energy decreases with the other energies increase. It was found that the projectile penetration is complete at 5 msec in terms of energy balance. The damage after penetration is clearly shown in Fig. 11. The dominant damage modes are fiber tensile failure and interface damage. The fiber tensile failure is local behavior accompanying with skin delamination, however, stringer flange delaminated conservatively when compared to test result. Thus, the skin/stringer interface is not well modeled in present model and should be modified to capture the skin/stringer interface damage properly.

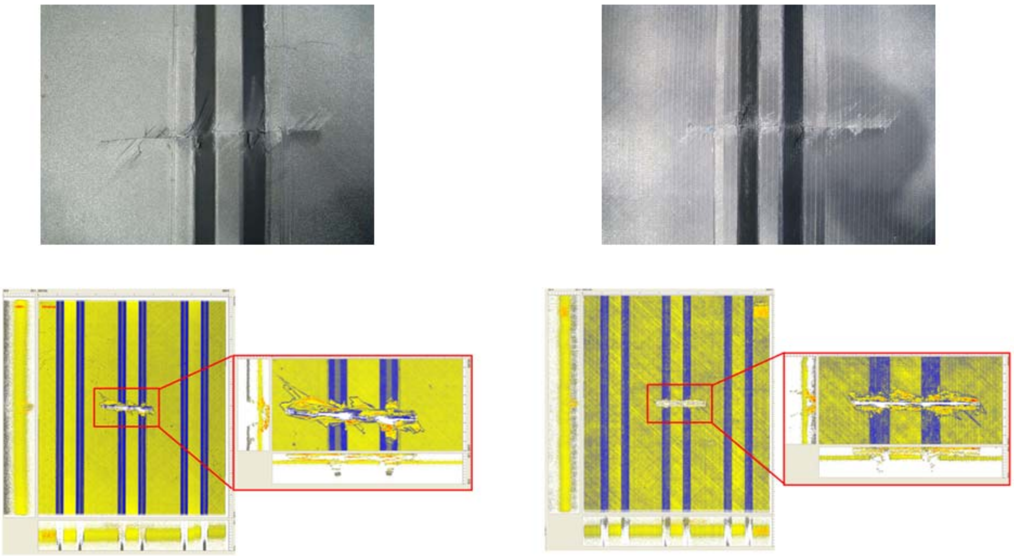

Fig. 6 Penetration damage and NDT result

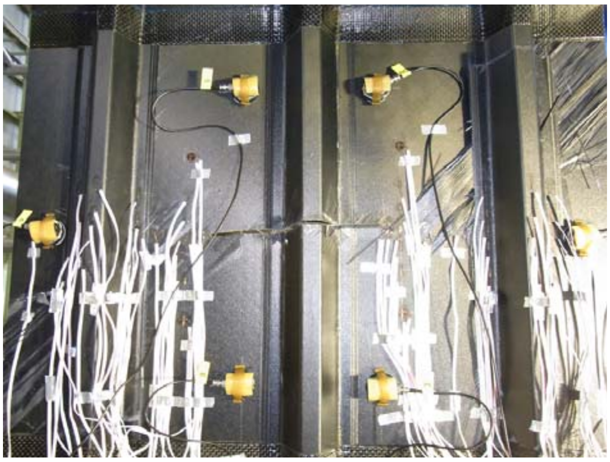

Fig. 7 Failure mode of prepreg panel

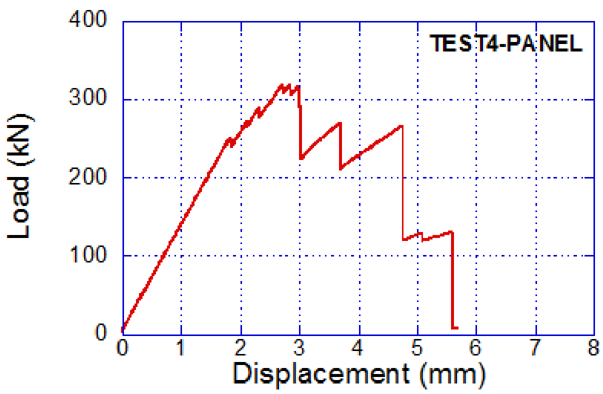


Fig. 8 Load-displacement curve for prepreg panel

finite element model has been generated because there has been a numerically difficulties to utilize the model above mentioned. Therefore, the model for tensile test has an ideal 200 mm long notched damage at the middle but with the same element constitution and material properties as blade penetration simulation. Figure 12 and 13 show the damage after tensile failure and load-displacement curve with relevant panel behavior for prepreg panel. The skin panel damage initiates from the both notch tips and propagates in the transverse direction, where dominant damage mode is tensile fiber failure. From this, it can be noticed that the large notch cracks on either side of the notch tips grow equally to the stringers. Then, the concentrated force in front of the crack-like damage tip causes damage in skin/stringer interface. Finally, the crack-like skin panel damage goes through the both stringers and the panel completely fails. This result qualitatively reveals that typical damage path is characterized by fiber breakage perpendicular to the crack tips to be followed by delamination propagation. The load-displacement curve follows the failure mechanism mentioned above, but, quantitatively, the simulation result doesn't show a reasonable agreement with the experimental data.

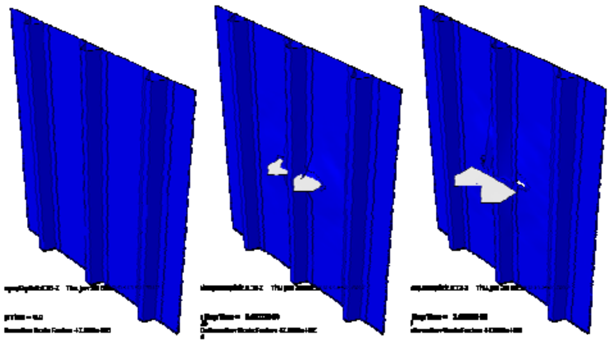

0 msec 0.5msec 1msec

Fig. 9 Progressive failure analysis result

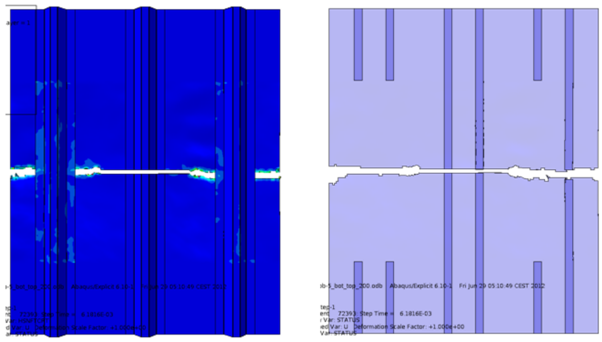

Fiber failure Interface damage

Fig. 12 Damage after tensile failure

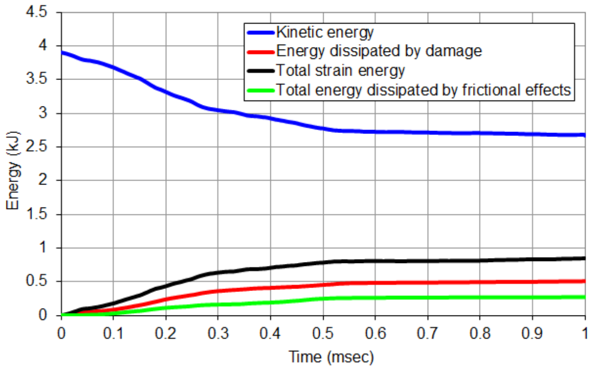


Fig. 10 Energy balance

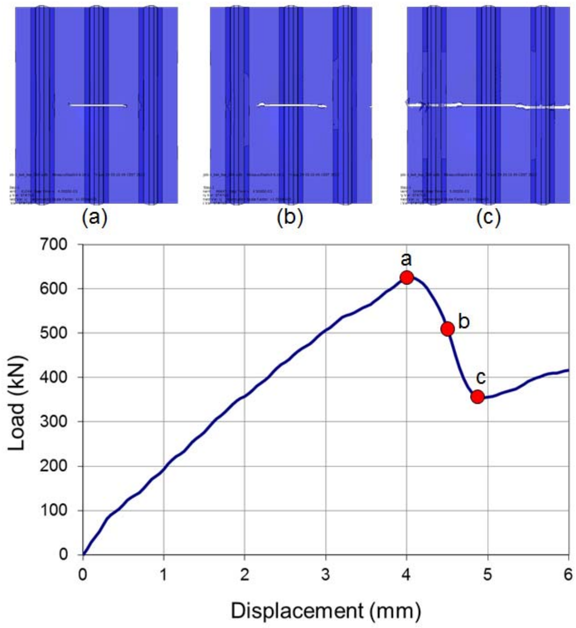


Fig. 13 Predicted load-displacement curve

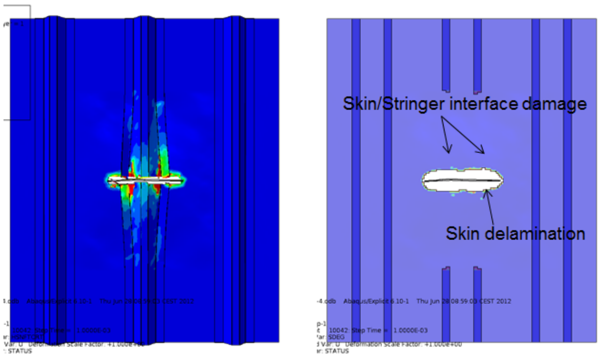


Fiber failure Interface damage

Fig. 11 Damage after penetration

## 5 Conclusions

Engine debris penetration tests were conducted to evaluate the large notch damage and residual strength of composite stiffened panel. The damage mechanism was also examined by progressive failure analysis based on Hashin's failure criteria and cohesive zone model. The influence of delamination on the progressing notched damage path and initial failure load of the panel are investigated. The results reveal that typical damage path is characterized by fiber breakage perpendicular to the crack tips to be followed by skin/stringer interface damage. The finite element model shows a potential capability to qualitatively predict the large notch damage and residual strength of the panel.

## References

[1] Lundin, S. and Mueller, R., Advanced Aircraft Materials, Engine Debris Penetration Testing, FAA report, DOT/FAA/AR-03/37, December 2005.
[2] Lundin, S., Engine Debris Fuselage Penetration Testing Phase II, FAA report, DOT/FAA/AR-01/27, II, August 2002.
[3] Seng, S., Manion, J. and Frankenberger, C., Uncontained Engine Debris Analysis Using the Uncontained Engine Debris Damage Assessment Model, FAA report, DOT/FAA/AR-04/16, September 2004.
[4] High Bypass Ratio Turbine Engine Uncontained Rotor Events And Small Fragment Threat Characterization Volume 1, AIA Project Report, January 2010.
[5] Fawcett, A., Damage Tolerance and the Composite Airframe, Commercial Aircraft Composite Repair Committee (CACRC) Meeting and Workshop for Composite Damage Tolerance & Maintenance, Tokyo, June 2009.
[6] Hashin Z, Failure Criteria for Unidirectional Fiber Composites, *Journal of Applied Mechanics*, Vol. 47, pp. 329–334, 1980.
[7] Hashin Z, and Rotem A, A Fatigue Criterion for Fiber-Reinforced Materials, *Journal of Composite Materials*, Vol. 7, pp. 448-464, 1973.

## Copyright Statement